

Temperature and thickness dependence at the onset of perpendicular magnetic anisotropy in FePd thin films sputtered on MgO(001)

C. Clavero,* J. M. García-Martín, J. L. Costa Krämer, G. Armelles, and A. Cebollada

Instituto de Microelectrónica de Madrid-IMM (CNM-CSIC), Isaac Newton 8-PTM, E-28760 Tres Cantos, Madrid, Spain

Y. Huttel

Instituto de Ciencia de Materiales de Madrid (ICMM-CSIC), 28049 Cantoblanco, Madrid, Spain

R. A. Lukaszew

Physics and Astronomy Department, University of Toledo, Mstop 111, 2801 W. Bancroft, Toledo, Ohio, USA

A. J. Kellock

IBM Almaden Research Center, 650 Harry Road, San Jose, California 95120, USA

(Received 23 January 2006; published 4 May 2006)

The onset of chemical order ($L1_0$ phase) and perpendicular magnetic anisotropy in FePd(001) thin films sputtered on MgO(001) at temperatures from room temperature to 700 °C and thickness between 1.4 and 22 nm are investigated. It is found that the formation of the FePd ordered phase exhibiting high perpendicular magnetic anisotropy ($L1_0$ phase with the c axis in the growth direction) is affected by a two-dimensional to three-dimensional growth mode transition with increasing deposition temperatures, hindering higher chemical ordering at moderate and high temperatures. For 22-nm-thick films, the ordered phase is only obtained in a narrow range of growth temperature centered at 450 °C. This fact, together with strong surface morphology dependence on the deposition temperature, determines the magnetic and magneto-optical properties of the studied system. No dependence of the ordering degree on film thickness is found for films with thicknesses of 3, 7 and 22 nm grown at 450 °C, with a constant value indicating that chemical ordering occurs since the early stages of growth and does not improve as the growth proceeds. The samples consist of chemically ordered nanostructures that range in size from 30 to 200 nm average diameter and 0.5–30 nm height as the film becomes thicker, and exhibit perpendicular magnetic anisotropy indicating that the c axis is parallel to the direction of growth. The largest coercive field (7 kOe) corresponds to the sample with nano-sized particles, and the coercivity drastically decreases down to 1 kOe as percolation sets in.

DOI: [10.1103/PhysRevB.73.174405](https://doi.org/10.1103/PhysRevB.73.174405)

PACS number(s): 75.75.+a, 75.70.Ak, 78.67.-n

I. INTRODUCTION

FePd and FePt binary alloys can form a chemically ordered phase ($L1_0$) that exhibits interesting properties such as high magnetic anisotropy ($K_u \sim 10^7$ J/m³ in FePt and $K_u \sim 9 \times 10^5$ J/m³ in FePd¹), and high magneto-optical (MO) response.^{2,3} The $L1_0$ chemically ordered phase is characterized by alternating pure Fe and Pd(Pt) atomic planes along the (001) direction, which imposes a tetragonal distortion with respect to the face centered cubic (fcc) cubic lattice, hence the appearance of high magnetic anisotropy (MA) along this direction. To achieve long range order (LRO), pure Fe and Pd(Pt) planes must extend over large enough and continuous flat regions, with a large lateral coherence and without defects [e.g., antiphase domain boundaries (APBs),^{1,4} where the stacking order of the atomic planes switches, thus breaking the chemical order]. To favor LRO in molecular beam epitaxy (MBE) or sputter deposited thin films of these alloys it is therefore important to grow the films at sufficient temperature to promote two-dimensional (2D) epitaxial growth mode, such that the atoms of each material can diffuse on the surface and adopt the correct position for the ordered phase. On the other hand, for technological applications such as ultrahigh density magnetic re-

ording media, it is necessary to obtain nano-sized magnetic structures, with high degree of chemical order and large MA (to overcome the superparamagnetic limit). Furthermore, these nanostructures must be magnetically uncoupled to minimize the interactions between them since ideally each nanostructure would constitute a bit of information whose magnetic state could be manipulated independently.⁵⁻⁷ Therefore, in this case three-dimensional (3D) growth mode would be preferable. One way to obtain these nanostructures is to promote a 3D growth using high temperature deposition,⁸ large lattice mismatch,⁹ or by exploiting the different surface energies between substrate and alloy layer.¹⁰ However, the simultaneous presence of high degree of chemical order and 3D growth is challenging since there are competing processes involved. Specifically, 3D growth mode will inhibit the formation of LRO over large lateral scales. It is therefore of fundamental and technological interest to determine the optimum deposition conditions needed to achieve chemical ordering and 3D growth simultaneously.

MgO(001) has been extensively used as substrate for the growth of epitaxial FePt and FePd alloy thin films, because it has very good crystalline quality and flat surface. It is worth noticing that it exhibits a high lattice mismatch with FePd ($\sim 10\%$) and the dielectric surface favors a 3D growth mode

for the metallic alloy.⁸ Most researchers use a buffer layer (e.g., Pd^{11,12} or Pt^{13,14}) prior subsequent growth of the alloy, to decrease lattice mismatch and the difference in surface energies. However, to favor 3D growth, the alloy can be grown directly onto the MgO(001) surface. Shima *et al.*¹⁵ studied the structure and magnetic behavior of FePt layers grown directly on MgO(001) by sputtering at different temperatures and with different thickness, obtaining granular films at high deposition temperatures with high degree of chemical order. The chemical order parameter S^4 is 1 for perfectly ordered films and 0 for disordered films, whereas in their case $S=0.95$. Regarding the growth of FePd directly on MgO(001), molecular beam epitaxy (MBE) has been the most commonly used deposition technique.^{16–19} For example, Kamp *et al.*¹⁹ studied the chemical ordering and morphology of FePd alloys deposited at temperatures ranging from room temperature (RT) up to 510 °C, obtaining a maximum value of $S=0.91$ at 350 °C. A comparison between the structure and the magnetic properties of systems fabricated using different deposition techniques, such as MBE and sputtering, is of special interest for technological applications, considering that these two techniques involve different energies thus affecting the growth mode, and sputtering might be preferred for industrial fabrication of high anisotropy binary alloys for new storage media. To our knowledge, this study for FePd thin films sputtered directly onto MgO(001) has not been reported so far. Thus, the aim of this work is to present our results on the epitaxy, morphology, structure, chemical ordering, magnetic and magneto-optical activity as a function of deposition temperature and thickness for FePd thin films sputter deposited directly onto MgO(001) surfaces.

It is shown below that the formation of the ordered phase that exhibits perpendicular magnetic anisotropy (PMA) is affected by a 2D–3D growth mode transition with increasing deposition temperature, and that a lower degree of chemical order is obtained compared to similar films grown using MBE. As a consequence, the ordered phase can only be obtained in a narrow temperature range around 450 °C. The morphology, structure, magnetic properties, domain structure and magneto-optical response of the samples is investigated as a function of the deposition temperature. Once the deposition temperature for maximum chemical order is determined (450 °C) the influence of the alloy film thickness on the chemical order and magnetic anisotropy is further investigated.

The paper is structured as follows: in Sec. II a brief description of the deposition and characterization techniques is given, in Sec. III the morphology, structure, magnetic anisotropy, domain structure, magneto-optical and spectral evolution of FePd thin films deposited at temperatures ranging from RT to 700 °C are described. Once the optimum growth temperature for chemical order formation is established, the thickness dependence on the films' properties is reported in Sec. IV, and finally Sec. V contains the main conclusions of this work.

II. EXPERIMENT

All the samples were grown in an ultrahigh-vacuum multichamber system equipped with sputtering and laser ablation

facilities (base pressure in the low 10^{-9} mbar range). The FePd alloy thin film growth was carried out using triode sputtering by co-deposition from Fe and Pd targets at 4×10^{-4} mbar Ar pressure. The FePd deposition rate of 0.24 Å/s was derived from x-ray reflectometry (XRR) measurements in a sample grown at RT and at the same conditions. The alloy film samples were grown at different temperatures and with different thickness. For the present studies, two series of samples were prepared: the first one consisting of 22-nm-thick FePd layers grown at temperatures ranging from RT to 700 °C, and a second set of FePd films with nominal thickness between 1.4 and 22 nm grown at 450 °C. Previous to the FePd films deposition, a 100-Å-thick MgO buffer layer was grown at 450 °C using normal incidence pulsed laser deposition from a monocrystalline MgO target on MgO(001) commercial substrates. This buffer layer improves the flatness and crystalline quality of the original substrate surface.²⁰ Once the FePd films were grown, a 2-nm-thick protective capping layer of MgO was deposited at RT in all cases. This dielectric capping layer is particularly convenient since it makes possible a simpler analysis of the magneto-optical properties of the system due to its transparent nature and eliminates potential modifications of the measured magnetic properties, specially in nanoparticle systems, where magnetically polarizable capping layers such as Pt and Pd have demonstrated to exert substantial effects.^{8,21}

Various techniques were used to investigate the alloy films, such as atomic force microscopy (AFM), x-ray diffraction (XRD) and XRR for the structural characterization, Rutherford backscattering (RBS) for the in-depth resolved chemical composition, and magnetic force microscopy (MFM), Kerr loops and Kerr spectroscopy for the magnetic and magneto-optical characterization. AFM and MFM images were obtained using a NanotecTM microscope in noncontact mode. Commercial probes from MikroMasch were used, with force constant and resonant frequency around 5 N/m and 150 kHz, respectively. In the case of MFM, the probes were coated with Cr 20 nm/Co 60 nm and magnetized along the axis of the pyramidal tip. Afterwards, the tip was scanned at constant lift height above the samples (typically 50 nm) and the phase shift, proportional to the force gradient, was measured. XRD and XRR experiments were performed in a standard four circles diffractometer with Cu $K\alpha$ radiation ($\lambda=1.5418$ Å) using the Bragg-Brentano configuration and 1/4 degree slits. RBS characterization was carried out in a NEC 3UH Pelletron instrument using 2.3 MeV He⁺ ions. Two detectors placed at 100 and 170° degrees from the forward direction of the incident beam (0°) were used. During the acquisition the sample was tilted 7° to the incident beam to minimize channeling in the crystalline substrate. The beam current used was 20 nA and 40 μC of charge was collected for each sample. Data reduction was performed using the RUMP (Cornell) software package.²² Using this technique the stoichiometry and thickness of two selected samples with 3 and 22 nm nominal thick FePd layers was confirmed. For the film with nominal thickness of 3 nm, the experimental thickness was measured to be 2.9 ± 0.3 nm and the chemical composition was found to consist of 49.6 ± 0.5 at. % in Fe and 50.1 ± 0.5 at. % in Pd, very close to the equiatomic stoichiometry. In the case of the nominal 22-nm-thick FePd

film, the experimental thickness found was 22.7 ± 1 nm and the concentrations 52.3 ± 0.5 at. % in Fe and 47.6 ± 0.5 at. % in Pd. The magnetic characterization was carried out measuring polar and transverse Kerr loops. Transverse loops were measured with a 633 nm HeNe laser system at RT at 45° incidence angle geometry, and the change in reflectivity was registered. In the case of polar Kerr loops 530 nm light in normal incidence was used and the Kerr rotation angle was measured. The magneto-optical (MO) activity of the samples was studied using polar Kerr spectra measured in a spectrometer described elsewhere,²³ in the spectral range from 1.4 to 4.3 eV.

III. DEPENDENCE ON THE DEPOSITION TEMPERATURE

The formation of the chemically ordered ($L1_0$) or the face centered cubic (fcc) disordered phase during alloy film growth depends strongly on the deposition temperature as shown in previous studies.^{1,14,24} Kamp *et al.*¹⁹ reported that the maximum ordering is achieved at 350°C in FePd alloys deposited using MBE on MgO(001), while Shima *et al.*¹⁵ reported the onset of FePt ordered phase at 500°C in films grown by sputtering on MgO(001), where the ordering increases with increasing temperature. In order to investigate this point in our deposition system a series of samples consisting of 22-nm-thick FePd films were grown using sputtering at temperatures ranging from RT to 700°C .

AFM images were taken for all the samples to investigate the dependence of the surface morphology on the deposition temperature. Figure 1 shows the morphological evolution of the surface for the samples grown at RT [Fig. 1(a)], 450°C [Fig. 1(b)] and 700°C [Fig. 1(c)], respectively. Clearly, a 2D–3D growth mode change is observed as the deposition temperature increases. The sample grown at RT is very flat with a root mean square (rms) roughness of 0.5 nm, whereas the samples grown at 450 and 700°C clearly exhibit a nanostructured surface morphology with presence of nanoparticles whose size depends on the deposition temperature. In the case of the sample deposited at 450°C , the particles have homogeneous size distribution with an average diameter of 200 nm and a mean height of 15 nm, with an average aspect ratio of roughly 10 to 1. On the other hand, for the sample grown at 700°C , a much less homogeneous distribution of particle sizes and shapes is observed. The surface is mostly populated with particles of irregular shape and 360 nm average diameter and height varying between 10 and 30 nm, and smaller particles are also observable between the large ones.

The crystalline structure, degree of chemical order and lattice parameters of the alloy films were determined using XRD. Symmetric and asymmetric XRD scans as well as rocking curves around the main reflection peaks were measured in all the samples. In order to determine the epitaxial relationship between the substrate and the FePd layer, the asymmetric FePd(220), and MgO(110) reflections were measured. This, together with the observation of the FePd(200) and MgO(200) reflections in the symmetric scans, allows us to establish the epitaxial relationship $[010] \times (001)\text{FePd} // [010](001)\text{MgO}$. In Fig. 2(a) high angle sym-

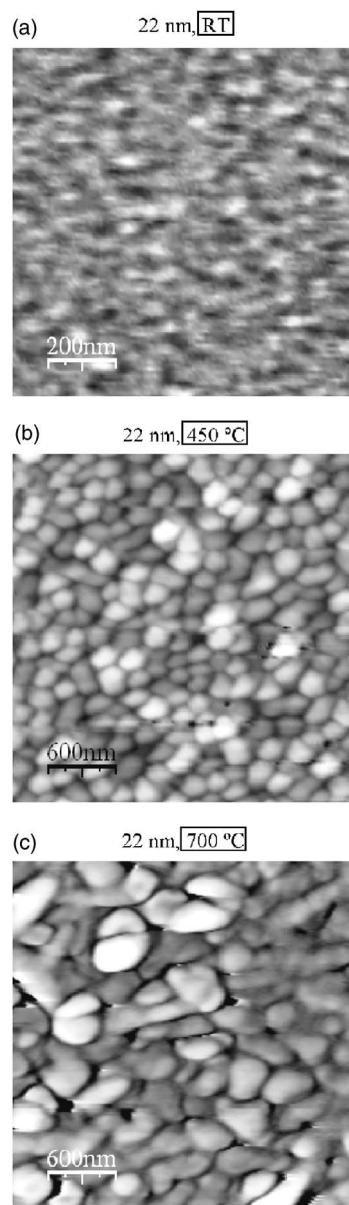


FIG. 1. AFM images showing the topography of 22-nm thick FePd films deposited at (a) RT, (b) 450°C and (c) 700°C are shown. Note the different scale in the image (a). The gray scale has been properly adjusted in each case between zero and the maximum height Z_{max} , with $Z_{\text{max}} = 1, 24$ and 52 nm for images (a), (b) and (c), respectively.

metric scans are shown, and the bulk position for the FePd chemically disordered fcc phase FePd(200) peak as well as the superstructure ordered bulk phase FePd(001) and (002) peaks¹ are indicated for reference. The FePd(001) peak is a forbidden reflection in fcc structures, and is therefore the characteristic signature of the presence of chemical order. It is only observed in the samples grown at 400, 450 and 500°C , indicating that tetragonal distortion only occurs in this narrow deposition temperature range. On the other hand, there is a clear evolution in the FePd(200) and (002) peaks as function of deposition temperature. The (002) alloy diffraction peak for samples grown at RT and 200°C is observed at

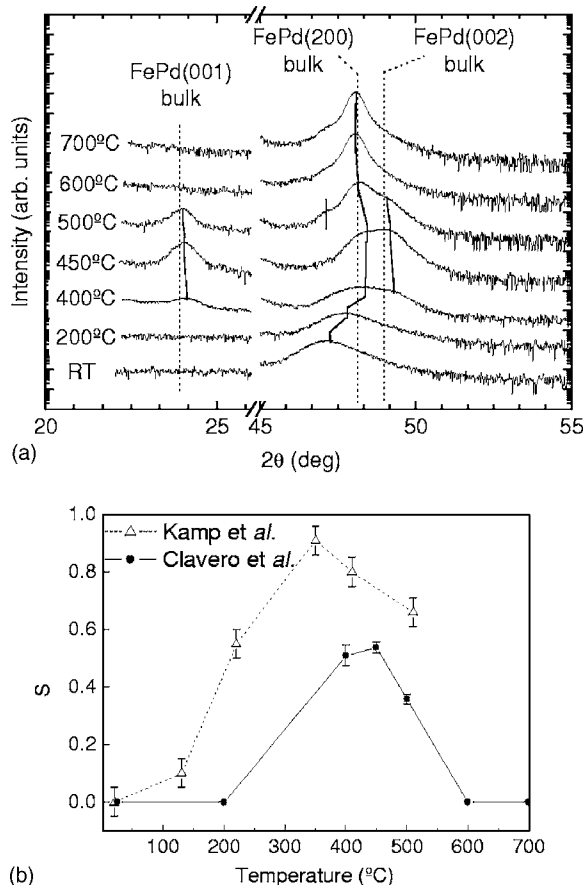


FIG. 2. Symmetric XRD scans for 22-nm-thick FePd films deposited at temperatures between RT and 700 °C. The presence of the peaks FePd(001) and (002) indicates the presence of $L1_0$ phase in samples grown at temperatures around 450 °C. (b) Chemical ordering parameter (S) evaluated for our samples grown by sputtering and for the samples reported by Kamp *et al.* (see Ref. 19) grown by MBE.

lower scattering angles than the bulk FePd(200) reflection, indicating a larger lattice parameter. The reflections corresponding to the three samples with some degree of chemical order are formed by the superposition of several peaks, basically one near the expected peak for bulk FePd(200) and another one near the bulk FePd(002) peak for 400 and 450 °C deposition temperatures, signifying multiphase growth and coexistence of ordered and disordered phases at these two temperatures. An additional third small peak at lower scattering angles and therefore corresponding to higher out of plane lattice parameter is observed for the sample grown at 500 °C, indicating the presence of a third FePd phase. Finally, at 600 and 700 °C, there are basically two reflections at the same scattering angle and corresponding to bulk, FePd(200) cubic phase: a narrow and intense one due to the large particles that were observed with AFM, and a weak and broad one, probably due to small particles between bigger ones observed in the AFM images.

Regarding the three samples that exhibit chemical order, we observe that the relative areas of the cubic phase FePd(200) and tetragonal ordered phase FePd(002) reflections evolve, the FePd(200) being larger than the (002) for

the samples grown at 400 and 500 °C, and the (002) larger than the (200) for the sample grown at 450 °C. This indicates that the disordered cubic phase is a majority phase for the 400 and 500 °C samples, whereas the $L1_0$ ordered phase is the majority phase for the 450 °C sample. An estimation of the relative disordered versus ordered phase occupations can be extracted from the relative areas of the two corresponding reflections. Ordered phase concentrations around 50% are found at 400 and 500 °C, whereas a higher concentration of 68% is found at 450 °C, supporting previous observations. On the other hand, it is also possible to calculate the one-dimensional chemical order parameter $S^{4,25}$ using the integrated areas of the FePd(001) and FePd(002) peaks. The calculated S values are plotted in Fig. 2(b) as a function of deposition temperature, and we note that the maximum order parameter is obtained at 450 °C ($S=0.54\pm 0.02$), clearly indicating that the ordered phase is only achieved for a narrow temperature range between 400 and 500 °C. For comparison, the values of S calculated by Kamp *et al.*¹⁹ for 30-nm-thick FePd films deposited by MBE directly on MgO(001) at temperatures between RT and 510 °C are also depicted in Fig. 2(b). In this case higher chemical ordering parameters are obtained at all temperatures, where the maximum value of $S=0.91\pm 0.05$ is observed at 350 °C. They also observed an increase of the roughness as the deposition temperature is increased, e.g., 0.3 nm for layers deposited below 420 °C, 1 nm for 420 °C and 5 nm in the sample grown at 510 °C. These roughness values are much lower than those obtained in our sputtered samples, where a variation in nanoparticles' height from 0.5 nm at RT to 15 nm at 450 °C and to 30 nm at 700 °C was observed. The different nature of the MBE and sputtering deposition techniques and obviously the multiphase (mixture of fcc and $L1_0$ phases) nature of our samples can explain the lower S values obtained in our case. On the other hand, the maximum chemical ordering reported by Kamp *et al.* at moderated temperature and also observed in our system (both peaking at around 400 °C) is in contrast with the evolution reported by Caro *et al.*¹⁴ in FePd grown on Pt(001)/MgO(001), where the ordering increases continuously with temperature (up to 600 °C which is the maximum temperature explored). Here, the metallic nature of the buffer layer used by these researchers, favors a 2D growth of the alloy film in a wider range of deposition temperatures and hence a higher chemical order.

A compilation of all the structural parameters extracted from the XRD measurements is presented in Table I: out-of-plane (c) and in-plane (a) lattice parameters for the FePd films are calculated from the position of the FePd(200) peaks and from the FePd(002) peaks in the samples with ordered phase as well as the position of the asymmetric FePd(220) diffraction peaks. A tetragonal distortion is observed in the ordered phase of the 450 °C sample, with a c/a ratio of 0.967 ± 0.005 , this value being identical to the one found in bulk FePd alloy.²⁶ More information about the grain size of the different phases can be extracted from the full width at half-maximum (FWHM) of the symmetric FePd(200) and (002) peaks, using the Scherrer's equation and a Gaussian fitting; the grain size is found to grow from 6 to 24 nm as the deposition temperature is increased. In the samples where

TABLE I. Lattice parameters, grain size, mosaic spread, chemical order parameter and concentration of $L1_0$ phase extracted from the XRD analysis of the series with different deposition temperatures.

	RT	200 °C	400 °C	450 °C	500 °C	600 °C	700 °C
Phase	fcc	fcc	fcc	$L1_0$	fcc	$L1_0$	fcc
$a(\text{Å})(\pm 0.001 \text{ Å})$	3.766	3.782	3.795	3.861	3.787	3.839	3.802
$c(\text{Å})(\pm 0.005 \text{ Å})$	3.853	3.809	3.762	3.721	3.764	3.711	3.778
Grain size ($\text{Å})(\pm 0.5 \text{ Å})$	60	65	53	90	118	110	178
Mosaic (deg) (± 0.01 deg)	3.71	3.92	4.24	4.52	1.31	1.31	0.58
S	0	0	0.50 ± 0.04	0.54 ± 0.02	0.36 ± 0.02	0	0
% $L1_0$ phase ($\pm 1\%$)	0	0	47	68	51	0	0

disordered and ordered phases coexist (400–500 °C) the grain size of the disordered phase continuously increases as a function of deposition temperature, whereas that of the ordered phase remains constant with a value oscillating between 9 and 11 nm, representative of a slower growth of the ordered grains as a function of deposition temperature compared to the disordered ones. In the 600 and 700 °C samples, the two Gaussians needed to properly fit the peaks, allow to quantify the out-of-plane crystalline coherence length of the particles with two characteristic sizes observed with AFM. The mosaic spread of the films which is related to the FWHM of the FePd(200) rocking curves was also calculated. It was found that it decreases from 3.7 to 0.48° with increasing deposition temperature, and it corresponds to improvement of the crystalline quality and alignment of the crystallite planes in the films. Finally, the chemical order parameter (S) and concentration of ordered phase are presented for each sample. A maximum chemical ordering ($S=0.54 \pm 0.02$) and concentration of $L1_0$ phase (68%) is achieved at 450 °C as previously described.

The magnetic anisotropy and magnetization reversal of the samples was studied using Kerr hysteresis loops both in polar and transverse geometry. The results are shown in Fig. 3, where polar loops appear on the left column with the magnetic field applied in the perpendicular direction and the corresponding transverse loops with the magnetic field applied along the in-plane FePd[100] and [110] directions on the right. In order to understand the behavior of the system we must consider that the two facts explained above are competing: on one hand, when the deposition temperature increases the sputtered thin films change their growth mode from 2D to 3D, as observed in similar systems;^{27,28} and on the other hand, a maximum amount of $L1_0$ phase is achieved at growth temperatures around 450 °C. The RT and 200 °C samples [Figs. 3(a), 3(b), 3(f), and 3(g)] show squared transverse Kerr loops exhibiting fourfold anisotropy, with [100] easy direction and [110] hard direction. Their polar loops have a large saturation field, corresponding to a continuous thin film with in-plane cubic anisotropy. At deposition temperatures around 450 °C the loops change considerably: in the polar Kerr loop a strong reduction of the saturation field and an increase of the coercive field up to 675 Oe [Fig. 3(c)] is clearly observed, all of this pointing to the presence of PMA consistent with ordered $L1_0$ phase with c axis parallel to the direction of growth. Moreover, in the transverse Kerr

measurements a reversible and minor in-plane loop is found [Fig. 3(h)], consistent also with the PMA of the film. For the sample grown at 500 °C the polar Kerr loop [Fig. 3(d)] is similar to that obtained for the sample grown at 450 °C, but with a larger saturation field and lower remanence and coercive field, indicative of a smaller PMA, and consistent with lower degree of chemical order. On the other hand, in the transverse loop [Fig. 3(i)] is not possible to saturate the sample with the fields available in our experimental setup, but a clear in-plane remanence and coercivity are observable, indicating that some part of the sample has in-plane magnetization. Finally, at 700 °C the polar Kerr loop [Fig. 3(e)] presents a large saturation field and zero remanence and coercive field, characteristic of an in-plane anisotropy system and consistent with the lack of chemical order for this sample. The corresponding transverse loop [Fig. 3(j)] is similar to that of the sample grown at 500 °C with even larger remanence. The rounded shapes of the transverse loops and the disappearance of the fourfold anisotropy for samples grown at 500 and 700 °C indicate a broad distribution of magnetization reversal switching fields, characteristic of noncontinuous nanoparticle structures,²⁹ also consistent with the morphology observed with AFM. In Fig. 3(k) the evolution of the coercive and saturation fields in the polar Kerr loops as a function of the deposition temperature is depicted. As was previously explained, the samples exhibiting higher ordering [Fig. 2(b)] and with larger amount of ordered phase show higher coercive field and a lower saturation field, both signatures of PMA. In this case the minimum saturation field is achieved in the sample grown at 450 °C, i.e., the sample with a maximum ordering. On the other hand, the maximum coercive field appears in the sample grown at 400 °C, in which the ordering degree was similar to the 450 °C sample. This small discrepancy is probably due to the fact that other factors can considerably affect the coercive field such as the morphology of the film, the size of the nanoparticles or the appearance of pinning centers that can delay the magnetization reversal.

Direct information about the magnetic domain structure was obtained by MFM. Figure 4 shows MFM images measured in the remanent state of two representative samples [450 °C Fig. 4(a) and 700 °C Fig. 4(b)]. Profiles along selected lines, where the measured signal (volts) has been transformed into force gradient (milliNewton/m) using the probe characteristics (i.e., force constant and resonant frequency) and the calibration curve (i.e., the linear evolution of

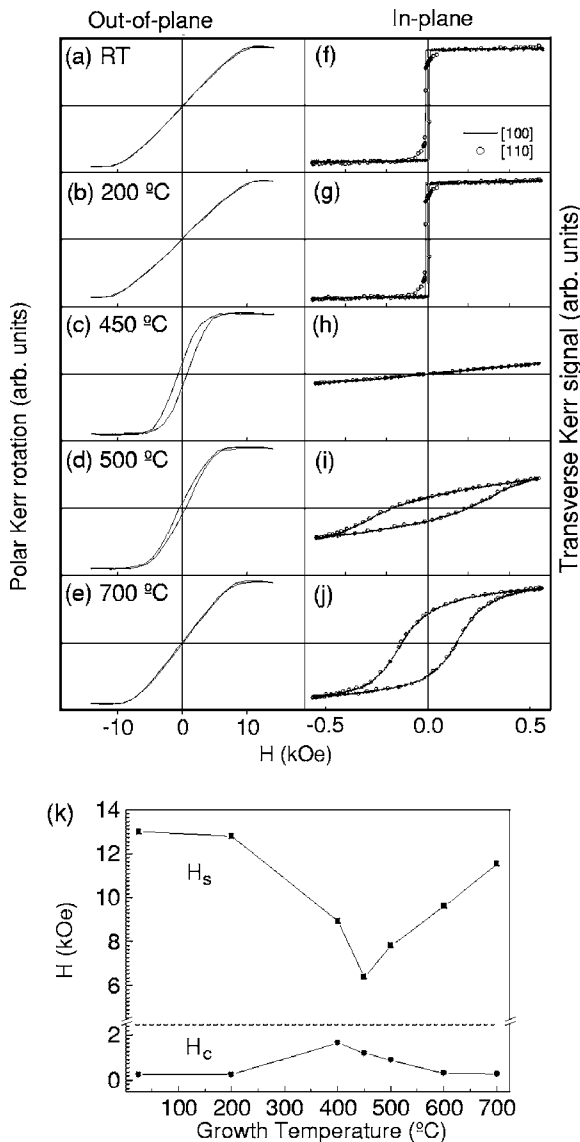


FIG. 3. (a)–(j) Evolution of the polar (left) and transverse (right) loops as a function of the growth temperature (RT–700 °C). For the transverse loops, two curves are shown, one obtained for the [100] direction (lines) and the other for the [110] direction (circles). The onset of $L1_0$ FePd ordered phase at temperatures around 450 °C and the 2D–3D growth mode transition determinate the loops. (k) Evolution of the saturation field (H_s) and coercive field (H_c) in the polar Kerr loops as a function of the growth temperature.

the phase versus the frequency around the resonance) are also shown in Fig. 4(c). The sample grown at 450 °C exhibits alternate dark and bright regions with high contrast (force gradient of about 20 mN/m): this is the distinctive characteristic of samples with PMA, where the dark and bright regions can be ascribed to magnetic domains with up and down magnetization, respectively.^{30,31} However, using similar tip and lift height in the MFM experiment, the sample grown at 700 °C only exhibits a weak contrast (one order of magnitude lower than in the previous case): this indicates that the magnetization lies mainly in the plane of the film but with a small perpendicular component that oscillates to re-

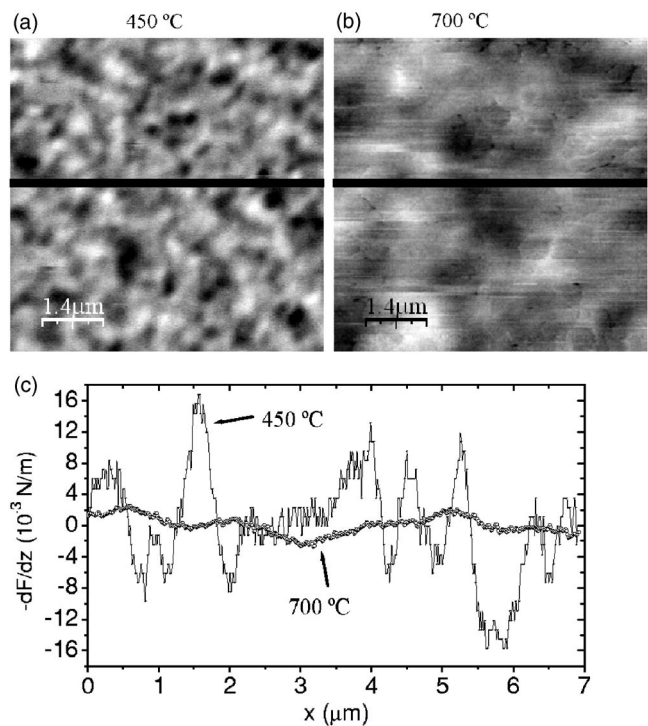


FIG. 4. (a) and (b): MFM images (size: $7 \times 7 \mu\text{m}^2$) of the samples grown at 450 and 700 °C. (c) Profiles along the black lines of the images.

duce the magnetostatic energy.³² The MFM observations agree with the magnetic evolution previously described by polar and transverse Kerr loops, where a transition from perpendicular to in-plane magnetic anisotropy occurs from 450 to 700 °C mediated by a strong reduction of the ordered phase at high temperatures.

In addition to changes in the magnetic anisotropy, the appearance of LRO is known to modify the MO activity in these binary alloy systems. We carried out polar Kerr spectroscopy measurements in the spectral range from 1.4 to 4.3 eV to identify these possible changes (Fig. 5). The measured spectra are characterized by a minimum between 2.5 and 3 eV whose position and intensity correlates with the degree of chemical order, appearing at higher photon energies for higher chemical order (450 °C sample), gradually shifting to lower photon energies and with higher intensity as the chemical order decreases. This finding has been previously reported in FePd² and FePt³³ alloys, where the position and intensity of the rotation spectra minimum placed at 2.5–3 eV was related to the degree of order in the alloy. In disordered alloys this minimum appeared at 2.5 eV, shifting toward higher energies (up to 3 eV) as the ordering increased in the system. In our results (Fig. 5), it can be observed that the position of the minimum follows the degree of ordering previously presented, and a shift towards higher energies is observed as the growth temperature is increased up to 450 °C, where the maximum ordering is achieved as demonstrated by XRD. At temperatures above 450 °C where the ordering degree was observed to decrease, the peak shifts back to lower energies. We can conclude that polar Kerr spectroscopy supports our XRD observations.

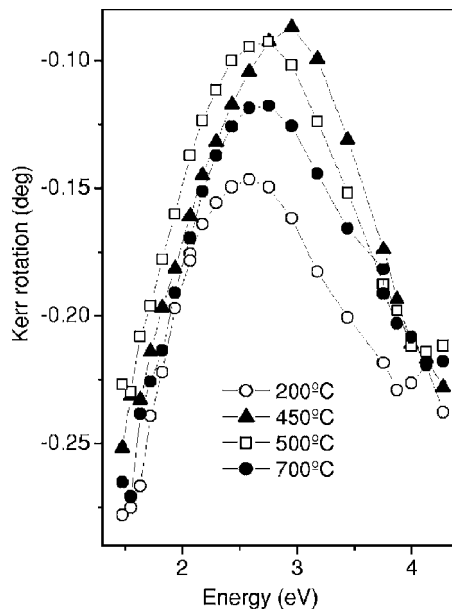


FIG. 5. Polar Kerr spectra for 22-nm-thick FePd films grown at temperatures ranging from 200 to 700 °C. The minimum shifts toward higher energies in the samples with higher chemical ordering.

IV. DEPENDENCE ON THE THICKNESS

In the first part of this work we have shown that it is possible to obtain PMA FePd alloys by direct growth on MgO(001) using sputtering. Our deposition temperature study showed that at a growth temperature of 450 °C it was possible to obtain structures with LRO and PMA despite the presence of some fcc fraction in the films. Another aspect of interest is to determine whether this LRO occurs from the early stages of growth or if it develops and improves as the layer becomes thicker. We therefore fabricated a second series of samples where the deposition temperature was 450 °C, i.e., the growth temperature that yielded maximum LRO, and the film thickness varied from 1.4 to 22 nm. Special care was taken in this series to optimize epitaxy of the FePd layers and to reduce the amount of fcc disordered phase found even in the samples exhibiting higher ordering degree in the previous series. To this end, better quality MgO substrates were obtained and improved by the growth of the MgO buffer layer.

The surface morphology evolution of the FePd films was investigated with AFM, as shown in Fig. 6. The granular nature observed in the first part of the work for this deposition temperature is obtained here as well. The observed nanoparticles grow in diameter and height as the thickness of the layer is increased. The 1.4-nm-thick FePd film [Fig. 6(a)] exhibits small nanoparticles with average in-plane diameter of 30 nm and 1 nm height (note: no capping layer was deposited in this sample in order to study the real shape of the nanoparticles and to avoid possible capping layer artifacts in the AFM measurements). As the thickness of the films increases the nanoparticles coalesce, becoming larger and taller: the 7-nm-thick FePd film [Fig. 6(b)] presents features with circular shape on the surface, with average in-plane diameter of 110 nm and 3 nm height. Finally, the previously

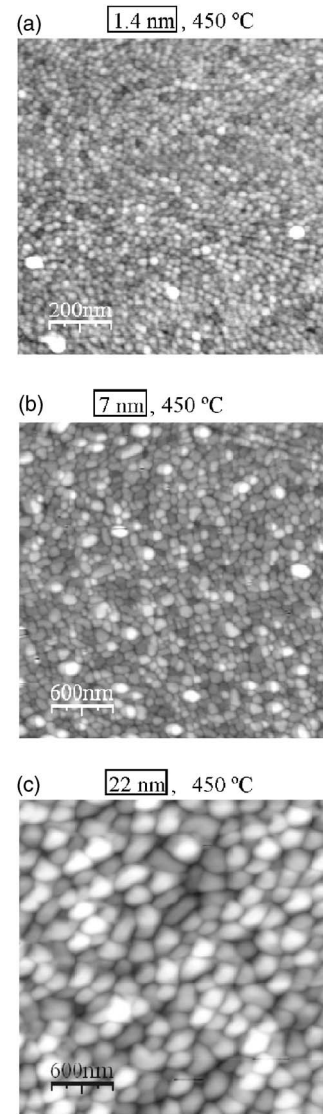


FIG. 6. AFM images showing the topography of FePd films deposited at 450 °C and with thickness (a) 1.4 nm (b) 7 nm and (c) 22 nm are shown. Note the different scale in the image (a). The gray scale has been properly adjusted in each case between zero and the maximum height Z_{\max} , with $Z_{\max}=3, 9,$ and 24 nm for images (a), (b) and (c), respectively.

described 22-nm-thick sample [Fig. 6(c)] presents features with average in-plane diameter of 200 nm and 15 nm height.

XRD analysis was performed to study the crystalline structure of the samples. Symmetric and asymmetric scans as well as rocking curves around the main reflection peaks were measured for all the samples. An epitaxial relationship $[010](001)\text{FePd}/[010](001)\text{MgO}$ was deduced in the same way as in the previous series. In Fig. 7 symmetric scans corresponding to the samples with a FePd 3-, 7- and 22-nm-thick layer are shown, the position of the bulk FePd(001), (002), (200) and (003) peaks is depicted as well. In all the symmetric scans the superlattice peaks FePd(001), (002), (003) and (004) of the $L1_0$ phase are found. In this series, the disordered FePd(200) peak is only slightly detected in the 7- and 22-nm-thick sample, indicating a much larger dominance

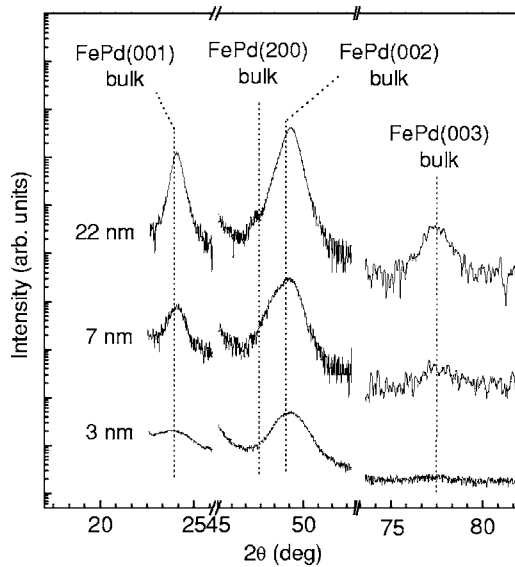


FIG. 7. Symmetric XRD scans for FePd films 3, 7 and 22 nm thick deposited at 450 °C. The superlattice peaks FePd(001), (002) and (003) are plotted.

of the ordered phase with respect to the disordered one as compared with the previous series. Again an estimation of the relative disordered versus ordered phase occupations was extracted from the relative areas of the (002) and (200) reflections. In this case the amount of ordered phase is close to 100% in the 3-nm-thick sample, 71% in the 7-nm-thick sample and 93% in the 22-nm-thick sample. These concentrations are higher than those obtained in the previous series, probably due to improved epitaxy. Also a slightly larger chemical order parameter S of around 0.6 was calculated for all the samples independent of their thickness. While there are no works on the development of S as a function of thickness in sputtered FePd films, Shima *et al.*¹⁵ found a constant value of S for FePt films 10–100 nm thick grown by sputtering on MgO(001) independently of the alloy thickness. Kamp *et al.*¹⁹ used transmission electron microscopy to study the FePd/MgO interface in MBE deposited structures. Their study indicates that the onset of epitaxial growth occurs immediately at the interface, with regular dislocations present in the first 3 nm to accommodate the 10% mismatch. This fact can explain the independence of the ordering on thickness in our case.

A compilation of the quantitative structural characterization by XRD of this second series is shown in Table II, where the lattice parameters c and a , grain size, mosaic spread, chemical order parameter and concentration of the ordered phase in the FePd films are shown. A tetragonal distortion is observed in all the samples with c/a ratio around 0.96, very close to the bulk value. In this case, the grain size of the ordered phase was extracted from the FWHM of the symmetric FePd(002) peaks and an increase with nominal thickness of the layers from 3 nm for the 3-nm-thick layer to 13 nm for the 22-nm-thick film was found (see Table II). The mosaic spread of the films, calculated from the FWHM of the rocking curves measured in the FePd(002) position, is found to decrease from 1.75° in the 3-nm-thick film to 1.3°

TABLE II. Lattice parameters, grain size, mosaic spread, chemical order parameter and concentration of $L1_0$ phase extracted from the XRD analysis of the series varying the FePd thickness grown at 450 °C.

	3 nm	7 nm	22 nm
Phase	$L1_0$	$L1_0$	$L1_0$
$a(\text{Å})(\pm 0.001 \text{ Å})$	3.856	3.847	3.847
$c\text{Å}(\pm 0.005 \text{ Å})$	3.707	3.714	3.697
Grain size $\text{Å}(\pm 0.5 \text{ Å})$	30	62	130
Mosaic (deg) (± 0.01 deg)	1.75	1.64	1.3
S	0.58 ± 0.04	0.67 ± 0.04	0.62 ± 0.06
% $L1_0$ phase ($\pm 1\%$)	100	71	93

in the 22-nm-thick film, indicating an increase of crystalline quality with increasing thickness. Therefore, from the XRD analysis it can be concluded that films grown at 450 °C have a chemical ordering independent of the thickness, and the crystalline quality improves in the thicker films.

The PMA nature of these chemically ordered structures is confirmed by polar Kerr hysteresis loops as shown in Fig. 8 (transverse loops were also measured but are reversible and minor for all these samples and they are not shown). Almost squared loops with large values of coercive fields are obtained. Remanence and coercivity increase with decreasing thickness, in close correlation with the morphology observed using AFM: 100% remanence, high coercive field of 7 kOe and saturation field of 15 kOe are observed in the 3-nm-thick film, corresponding to a system with strong PMA [Fig. 6(a)]. As the thickness of the layers is increased, the nanoparticles become larger and coalesce [Fig. 6(b) and 6(c)], decreasing the coercive field up to 1 kOe and the saturation field up to 7 kOe in the 22-nm-thick sample. This decrease of the coercive field as the thickness of the layer is increased has been previously observed in FePt films by Shima *et al.*,^{15,34} and can be ascribed to the morphology change of the films from nanoparticulate to continuous layer. In Shima's samples the coercive field was 40 kOe for the thinner one (10 nm) and of 30 kOe in the 20-nm-thick sample, drastically decreasing the coer-

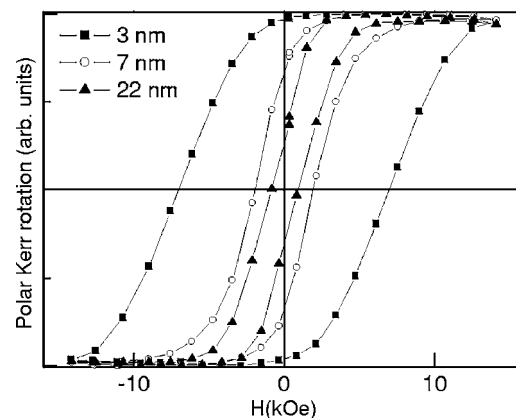


FIG. 8. Polar Kerr loops for FePd films 3, 7 and 22 nm thick deposited at 450 °C.

civity with percolation of the nanoparticles for thickness above 45 nm.

V. CONCLUSIONS

We have studied the formation of chemically ordered $L1_0$ phase and the magnetic anisotropy in equiatomic FePd alloy films sputtered on MgO(001) substrates as a function of the deposition temperature and thickness of the layers. In 22-nm-thick FePd films the $L1_0$ ordered phase exhibiting PMA is only achieved in a narrow temperatures range centered in 450 °C, with a maximum chemical order parameter $S = 0.54 \pm 0.02$. We speculate that the 2D–3D growth mode transition and the mixture of $L1_0$ and fcc found in the samples hinders LRO and prevents further chemical ordering. The magnetic behavior of the samples is determined by the formation of ordered phase with PMA at moderated temperatures and by the morphological evolution from 2D to 3D. The magnetic domain structure and the polar Kerr spectra support the order-disorder change and the out-of-the-plane magnetization switch at temperatures around 450 °C.

In samples grown at 450 °C and with thickness ranging from 3 to 22 nm a constant chemical order parameter around $S = 0.6$ is calculated, indicating that the chemical order process starts during the very first stages of growth. Different nanoparticle sizes were obtained (30–200 nm average diameter and 0.5–30 nm height) exhibiting perpendicular magnetization, with a 7 kOe coercive field for the sample with smaller nanoparticles, decreasing the coercivity considerably down to 1 kOe as percolation emerges.

ACKNOWLEDGMENTS

This work was partially financed by the Spanish Commission of Science and Technology and Comunidad de Madrid. C.C. acknowledges the Ministerio de Educación y Ciencia and FPI program for financial support. J.M.G.-M. and Y.H. acknowledge the Consejo Superior de Investigaciones Científicas (CSIC) and Ramón y Cajal program for financial support. This work was also partially supported by NSF-DMR (Grant No 0355171), the American Chemical Society (ACS-PRF-41319-AC10) and the Research Corporation.

*Electronic address: cesarcl@imm.cnm.csic.es

- ¹A. Cebollada, R. F. C. Farrow, and M. F. Toney, *Magnetic Nanostructures*, edited by H. S. Nalwa (American Scientific, Los Angeles, 2002).
- ²G. Armelles, D. Weller, B. Rellinghaus, P. Caro, A. Cebollada, and F. Briones, *J. Appl. Phys.* **82**, 4449 (1997).
- ³T. Katayama, T. Sugimoto, Y. Suzuki, M. Hashimoto, P. De Haan, and J. C. Lodder, *J. Magn. Magn. Mater.* **104**, 1002 (1992).
- ⁴B. E. Warren, *X-Ray Diffraction* (Dover, New York, 1990), p. 216.
- ⁵D. Weller and A. Moser, *IEEE Trans. Magn.* **35**, 4423 (1999).
- ⁶S. Sun, C. B. Murray, D. Weller, L. Folks, and A. Moser, *Science* **287**, 1989 (2000).
- ⁷S. Sun, E. E. Fullerton, D. Weller, and C. B. Murray, *IEEE Trans. Magn.* **37**, 1239 (2001).
- ⁸E. Navarro, Y. Huttel, C. Clavero, A. Cebollada, and G. Armelles, *Phys. Rev. B* **69**, 224419 (2004).
- ⁹T. Seki, T. Shima, K. Takahashi, Y. Takahashi, E. Matsubara, Y. K. Takahashi, and K. Hono, *J. Appl. Phys.* **96**, 1127 (2004).
- ¹⁰S. H. Overbury, P. A. Bertrand, and G. A. Somorjai, *Chem. Rev. (Washington, D.C.)* **75**, 547 (1975).
- ¹¹D. Halley, B. Gilles, P. Bayle-Guillemaud, R. Arenal, A. Marty, G. Patrat, and Y. Samson, *Phys. Rev. B* **70**, 174437 (2004).
- ¹²G. Beutier, A. Marty, K. Chesnel, M. Belakhovsky, J.-C. Toussein, B. Gilles, G. van der Laan, S. Collins, and E. Dudzik, *Physica B* **345**, 143 (2004).
- ¹³J. L. Menéndez, P. Caro, A. Cebollada, F. Briones, D. García, M. Vázquez, A. Hernando, and J. A. García, *J. Magn. Magn. Mater.* **206**, 1 (1999).
- ¹⁴P. Caro, A. Cebollada, F. Briones, and M. F. Toney, *J. Cryst. Growth* **187**, 426 (1998).
- ¹⁵T. Shima, K. Takahashi, Y. K. Takahashi, K. Hono, G. Q. Li, and S. Ishio, *J. Magn. Magn. Mater.* **266**, 171 (2003).
- ¹⁶P. Kamp, M. Belakhovsky, C. Boeglin, H. A. Dürr, G. van der Laan, P. Schille, A. Rogalev, J. Goulon, V. Gehanno, A. Marty, and B. Gilles, *Physica B* **248**, 127 (1998).
- ¹⁷E. Dudzik, S. S. Dhesi, H. A. Dürr, S. P. Collins, M. D. Roper, G. van der Laan, K. Chesnel, M. Belakhovsky, A. Marty, and Y. Samson, *Phys. Rev. B* **62**, 5779 (2000).
- ¹⁸O. Klein, Y. Samson, A. Marty, S. Guillous, M. Viret, C. Fermon, and H. Alloul, *J. Appl. Phys.* **59**, 6781 (2001).
- ¹⁹P. Kamp, A. Marty, B. Gilles, R. Hoffmann, S. Marchesini, M. Belakhovsky, C. Boeglin, H. A. Dürr, S. S. Dhesi, G. van der Laan, and A. Rogalev, *Phys. Rev. B* **59**, 1105 (1999).
- ²⁰C. Martínez Boubeta, C. Clavero, J. M. García-Martín, G. Armelles, A. Cebollada, L. Balcells, J. L. Menéndez, F. Peiró, A. Cornet, and M. F. Toney, *Phys. Rev. B* **71**, 014407 (2005).
- ²¹E. Navarro, Y. Huttel, C. Clavero, G. Armelles, and A. Cebollada, *Appl. Phys. Lett.* **84**, 2139 (2004).
- ²²L. R. Doolittle, *Nucl. Instrum. Methods Phys. Res. B* **15**, 227 (1986).
- ²³W. S. Kim, M. Aderholz, and W. Kleemann, *Meas. Sci. Technol.* **4**, 1275 (1993).
- ²⁴M. F. Toney, W. Y. Lee, J. A. Hedstrom, and A. Kellock, *J. Appl. Phys.* **93**, 9902 (2003).
- ²⁵A. Cebollada, D. Weller, J. Sticht, G. R. Harp, R. F. C. Farrow, R. F. Marks, R. Savoy, and J. C. Scott, *Phys. Rev. B* **50**, 3419 (1994).
- ²⁶W. Pearson, *Handbook of Lattice Spacings and Structures of Metals* (Pergamon, New York, 1958).
- ²⁷M. G. Kim, S. C. Shin, and K. Kang, *Appl. Phys. Lett.* **80**, 3802 (2002).
- ²⁸Y. K. Takahashi, K. Hono, T. Shima, and K. Takahashi, *J. Magn. Magn. Mater.* **267**, 248 (2003).
- ²⁹F. Cebollada, A. Hernando-Mañeru, A. Hernando, C. Martínez-Boubeta, A. Cebollada, and J. M. González, *Phys. Rev. B* **66**, 174410 (2002).
- ³⁰V. Gehanno, A. Marty, B. Gilles, and Y. Samson, *Phys. Rev. B*

- 55**, 12552 (1997).
- ³¹A. Asenjo, J. M. García, D. García, A. Hernando, M. Vázquez, P. A. Caro, D. Ravelosona, A. Cebollada, and F. Briones, *J. Magn. Mater.* **196-197**, 23 (1999).
- ³²A. Asenjo, D. García, J. M. García, C. Prados, and M. Vázquez, *Phys. Rev. B* **62**, 6538 (2000).
- ³³S. Mitani, K. Takanashi, M. Sano, H. Fujimori, A. Osawa, and H. Nakajima, *J. Magn. Mater.* **148**, 163 (1995).
- ³⁴T. Shima, T. Takanashi, Y. K. Takahashi, and K. Hono, *Appl. Phys. Lett.* **81**, 1050 (2002).